J Nanostruct 13(3): 806-820, Summer 2023

RESEARCH PAPER

Synthesis of $CeVO_4$:Dy^{3+} Nanoparticles as Down Converter and Its Application for Efficiency Enhancement in Dye-Sensitized Solar Cells

Zohreh Chamanzadeh [1], Nafiseh Sharifpour [2], Mostafa Zahedifar [3], Mahdi Madani [2]*

[1] *School of physics, Damghan University, Damghan, Iran*

[2] *School of Electrical and Computer Engineering, University of Tehran, Tehran, Iran*

[3] *Physics Department, University of Kashan, Kashan, Iran*

ARTICLE INFO

Article History:
Received 13 March 2023
Accepted 20 June 2023
Published 01 July 2023

Keywords:
$CeVO_4$
Dye sensitized Solar Cell
Electrophoresis
Luminescent
Nanoparticles

ABSTRACT

For the first time, the application of $CeVO_4$:Dy^{3+} luminescent film as down converter for efficiency enhancement in Dye Sensitized Solar Cell (DSSC) was studied through two ways, inside and outside the DSSC in order to increase the sun light harvesting and achieving increased DSSC efficiency. $CeVO_4$ nanoparticles (NPs) were synthesized by hydrothermal method at various reaction times and temperatures and then characterized by X-ray diffraction (XRD), photoluminescence (PL), Field-emission scanning electron microscopy (FE-SEM), transmission electron microscopy (TEM) and UV-Vis absorption spectroscopy. The $CeVO_4$:Dy^{3+} NPs with different molar ratios of Dy^{3+} ion were synthesized and characterized by PL spectroscopy. Photoelectrodes (PEs) of DSSC were produced by electrophoresis deposition (EPD). A film of these luminescent NPs on the back surface of the PE of DSSC resulted in increased DSSC efficiency by 8.05% compared to that of the cell based on uncoated photoelectrode, while using them as precursor in preparation PE improved the cells efficiency by 5.56%. The improvement can be attributed to the down conversion effect of $CeVO_4$:Dy^{3+} nanoparticles.

How to cite this article
Chamanzadeh Z., Sharifpour N., Zahedifar M., Madani M. Synthesis of $CeVO_4$:Dy^{3+} Nanoparticles as Down Converter and Its Application for Efficiency Enhancement in Dye-Sensitized Solar Cells. J Nanostruct, 2023; 13(3):806-820. DOI: 10.22052/JNS.2023.03.021

INTRODUCTION

The global request for energy is approximated to double by the year 2050, because of the ongoing industrialization and population growth [1, 2]. Sunlight is a free, clean and unlimited source of energy that can be obtained by photovoltaic (PV) cells to generate electricity [3-5]. However, the biggest factors of cost and efficiency of solar energy production are prevented the environmentally friendly and sustainable technology [6]. Dye sensitized solar cell (DSSC) is one of the promising third generation photovoltaic technologies [7-9].

Due to highly efficient, simple to fabricate and low-cost of Dye-sensitized solar cells, they are currently attracting widespread scientific and technological interest alternative to conventional photovoltaic devices [10-12]. Conventional DSSC is composed of a wide band gap semiconductor (TiO_2) as photo anode, Ru complex dye as sensitizer, an iodine-based electrolyte and Pt counter electrode [13]. It's principle of operation is similar to the photosynthesis process. In a DSSC, dye molecule absorbs incident photons, and then injects an electron into the conduction band of the

* *Corresponding Author Email: z.chamanzadeh@du.ac.ir*

nanocrystalline TiO_2 film upon optical excitation and is subsequently regenerated back to the ground state by electron donation from a redox couple presents in the electrolyte [14, 15].

However, the power conversion efficiency of DSSCs is still limited [16]. There are two issues encountering UV radiation: (i) exposure to UV radiation has been found to be deleterious for DSSCs because the dye will be rapidly photo oxidized under UV illumination. One strategy to avoid the UV radiation is using an additional UV filter specially coated to absorb ultraviolet rays, however, the use of UV filter wastes large part of the solar energy [17, 18]. And (ii) the photo anode has a maximum absorption in the visible region of the incident solar irradiation, in other words, approximately 50% of solar irradiation energy in the ultraviolet and infrared regions is not utilized. This restriction is one problem that limits the efficiency enhancement [19, 20]. To increase light absorption and modify the conversion efficiency, many research efforts have been focused on modifying the anode of DSSCs for matching the spectral response to the solar spectrum [20-22].

Therefore, a promising approach to overcome the fundamental problem of energy losses is to convert UV photons into longer wavelength photons (down conversion) by assistance with rare-earth (RE) ions in solid-state materials. The conversion layer exhibits attractive prospect as a UV filter to increase its stability, moreover the UV radiation absorbed by DC nanoparticles (NPs) could be down-converted into visible light which can be reabsorbed by dye in DSSCs [23, 24].

Lanthanide-based NPs have attracted significant attention for its ability to gather the UV-blue part of solar spectrum [25-27]. Nanostructured rare earth orthovanadates, RVO_4 (R = La, Ce, Nd, Gd, Eu, Sm) have been widely studied due to their important properties [28-31]. They have been used in catalysis, optical polarizer, gas sensors, lithium intercalated electrode, laser host materials, solar cells, thin film phosphors, unusual magnetic materials and luminescent properties [32, 33]. Generally, the RVO_4 structure has two polymorphs, a monoclinic (m-) monazite-type and a tetragonal (t-) zircon type. The phase of the individual RVO_4 is dependent upon the ionic radii of rare earth elements. However, $CeVO_4$ is placed in between the boundary of the monazite and zircon types [32]. In fact, the formation of RVO_4 phase (R=Sm and Ce) results in interaction between the nuclear spin of the V atom and unpaired 4f electron of R. Fermi contact interaction could be involved with a transfer of the unpaired 4f electron of the R ions to the orbital on V atom and hence a slight chemical shift to a higher binding energy (shifted 0.3- 1.3 eV) of Sm 3d, Ce 3d, and V 2p of RVO_4 NPs compared with that of Sm_2O_3, CeO_2, and V_2O_5 NPs. As a result, V and R possess a valence of +5 and +3, respectively, in the RVO_4 lattice [34].

In this work, the $CeVO_4$ and $CeVO_4$:Dy^{3+} NPs were prepared for the first time via the hydrothermal method using non-ionic surfactant Brig 35. The morphology, crystal structure and optical properties of the as-prepared nanoparticles were studied. For the first time in our knowledge, we report the application of $CeVO_4$:Dy^{3+} NPs in the structure of DSSC as a down converter. Results show that $CeVO_4$:Dy^{3+} NPs could absorb UV light and down-convert it to visible light and improve the current density of DSSC.

MATERIALS AND METHODS

Preparation of $CeVO_4$ NPs

All the chemical reagents include Cerium (III) nitrate hexahydrate ($Ce(NO_3)_3 \bullet 6H_2O$, Aldrich), Dysprosium (III) nitrate pentahydrate ($Dy(NO_3).5H_2O$, Alfa Aesar), ammonium metavanadate (NH_4VO_3, Merck), DI Water (Merck), and Brij 35 (Merck) were of analytical grade. In the first step, $CeVO_4$ NPs were synthesized by

Table 1. Prepared samples of $CeVO_4$.

Sample no.	Time (h)	Temperature (°C)
1	12	120
2	12	140
3	12	160
4	12	180
5	10	140
6	16	140
7	24	140

a simple hydrothermal method. First 1 mmol $Ce(NO_3)_3 \bullet 6H_2O$ and Brij 35 with equal weight ratios were dissolved in 20 ml deionized water, then the second solution was prepared by dissolving 2.56 mmol NH_4VO_3 in 20 ml deionized water, and this solution was slowly added to the initial solution while was stirred for 15 min. The final solution was transferred into 50 ml teflon-lined stainless-steel autoclave and the reaction was completed in a hydrothermal digestion system at various temperature and time as shown in Table 1. The obtained precipitate washed with distilled water for several times and then dried at 90 ˚C for 4 h. Then, $CeVO_4$:Dy^{3+} nanocrystals with different molar ratios of Dy^{3+} ion were synthesized at 140 ˚C for 12 h. subsequently, the prepared sample annealed at temperatures 300, 500, 700 and 900 ˚C in air for 1 h.

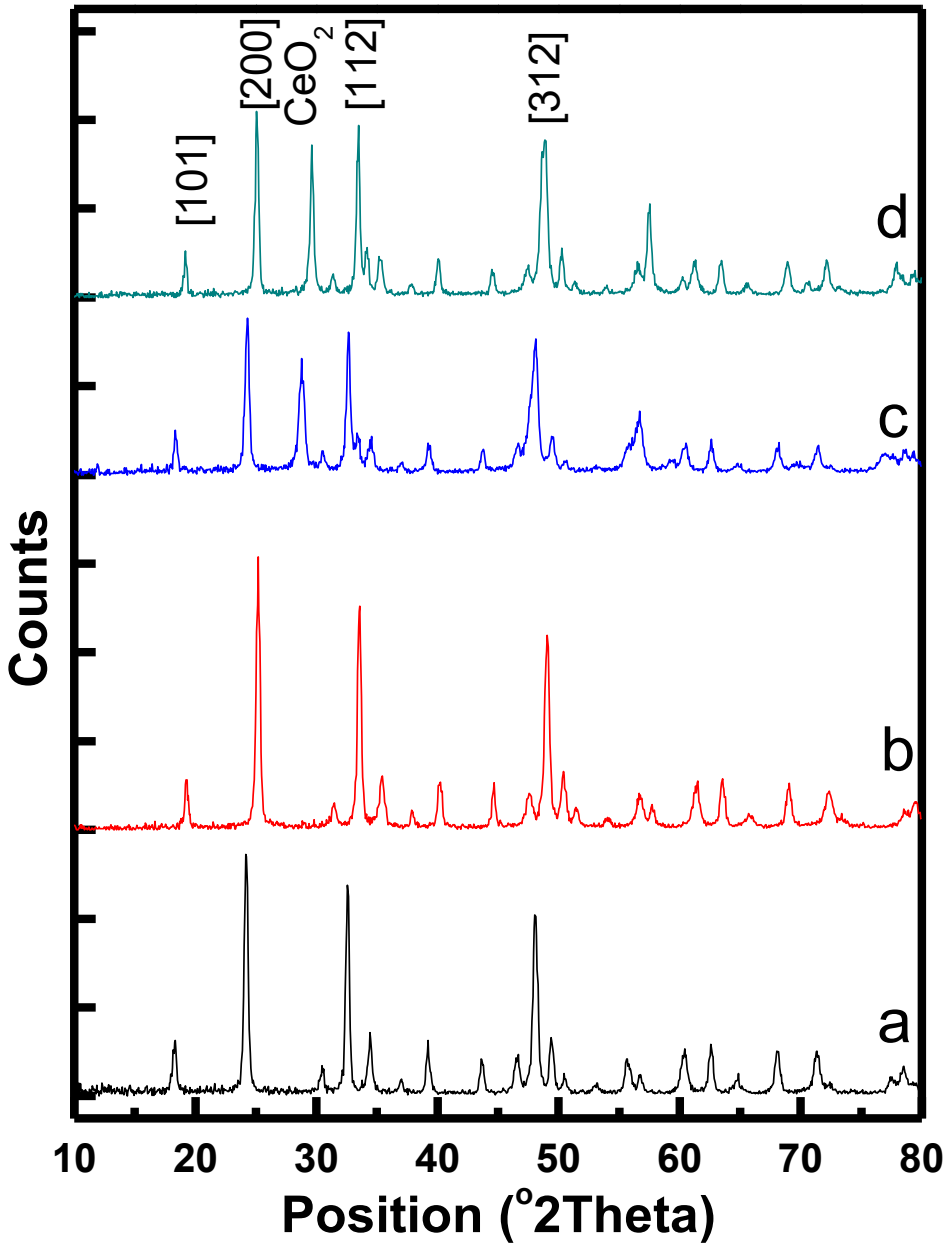

Fig. 1. XRD patterns of as prepared samples at different temperature. a) 120, b) 140, c) 160, d) 180°C.

Characterization

The crystal structure of the products was characterized by a Philips- X'pertpro, X ray diffractometer (XRD) using Ni-filtered Cu Ka radiation at scan range of 2θ (10–80). The morphology was investigated using a Field-emission scanning electron microscope (FE-SEM, Mira 3-XMU) and Energy Dispersive Analysis of X-ray (EDAX) was taken by MIRA 3 FEG Tescan. Transmission electron microscope from JEM-2100 operating at 200 kV was used to observe the Transmission electron microscopy (TEM) images. Room temperature photoluminescence (PL) properties of samples was studied on a Perkin-Elmer (LS 55) fluorescence spectrophotometer. The UV–Vis absorption spectra (UV–Vis) was measured under the diffuse reflectance mode using Shimadzu UV–Vis scanning spectrometer. The current-voltage characterizations of the DSSCs were measured by solar simulator (Luzchem) and IVIUMSTAT (IVIUM) under AM 1.5 illumination (100 $mWcm^{-2}$). Measurement of thickness of

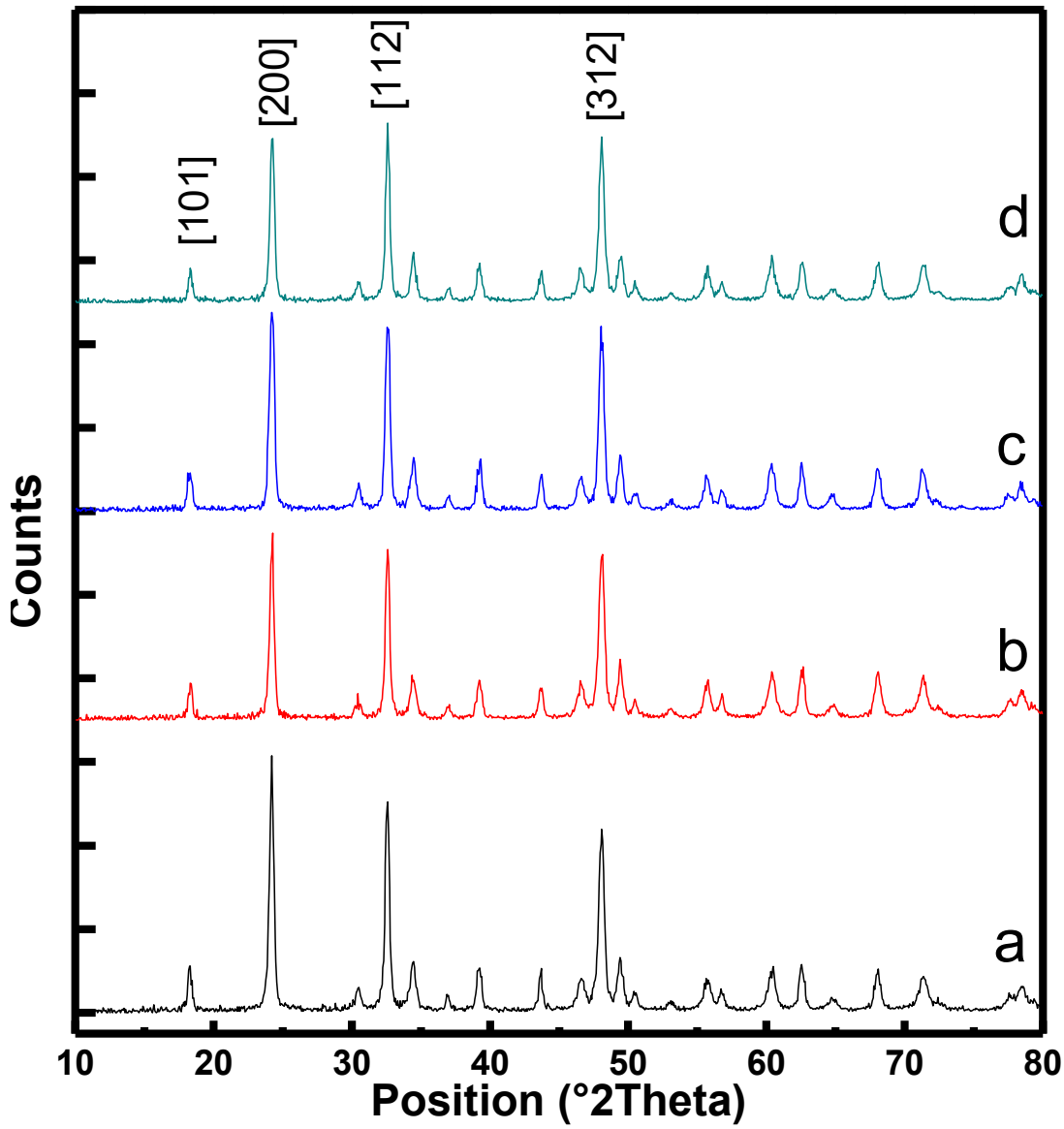

Fig. 2. XRD patterns of as prepared samples at different time at constant temperature of 140°C. a) 12, b) 10, c) 16, d) 24 h.

working electrode was done using 3d Optical Microscope Nanofocus.

RESULTS AND DISCUSSION

Morphology and characterization

XRD patterns and FE-SEM analyses were used to optimize the time and temperature of synthesis. Fig. 1 shows the XRD patterns of the as-prepared samples at different temperatures a) 120, b) 140, c) 160, d) 180°C. Fig. 1(c,d) show the XRD patterns of $CeVO_4$ along with an additional phase of CeO_2 which are fairly fitted with monazite structure JCPDS card No. 84-1457 and 43-1002, respectively. Fig. 1(a,b) shows the XRD patterns of $CeVO_4$ NPs. All diffraction peaks of $CeVO_4$ nanocrystals are in good agreement with the standard pattern (JCPDS 84-1457). Moreover, no other impurity phases were found in the prepared samples at 120 and 140 ˚C. However, as is evident, background radiation of XRD pattern for sample produced at 140 °C is less, so, this was selected as the optimum temperature. Bragg's reflections from this sample were observed in XRD pattern at 2θ values of 18, 24, 32, 48 representing [101], [200], [112],

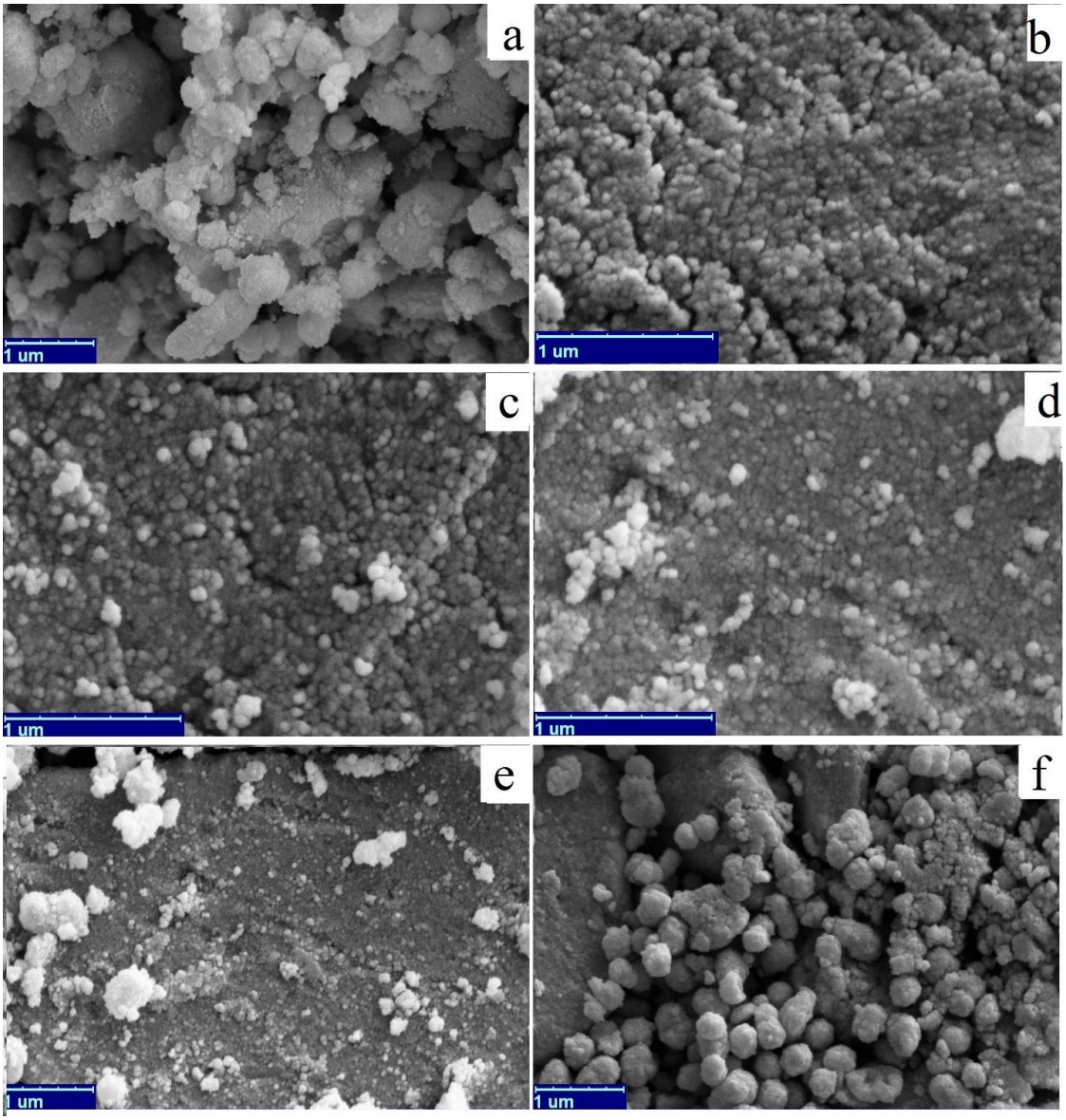

Fig. 3. SEM images of $CeVO_4$ samples a-f which relate to table 1as: a) 1, b & c) 2, d) 5, e) 6, f) 7

[312] planes of tetragonal phase with the lattice constants of a=b= 7.354 Å and c= 6.488 Å. Fig. 2 shows the XRD patterns of $CeVO_4$ NPs at different times with a constant temperature of 140 °C. All diffraction peaks of the $CeVO_4$ are compatible with the standard pattern (JCPDS 84-1457). In addition, no more impurity phases were found in the products. As shown, the sharpest main peak in XRD patterns belong to the samples produced at 140 °C for 12 h. The influences of temperature and time on the morphology of $CeVO_4$ nanocrystals were also studied.

Fig. 3 shows the FE-SEM images of as prepared samples specified as a-f in accordance with Table 1. It is obvious that the produced NPs are uniform and the morphology is nanosphere with the diameter ranging from 35-70 nm. Changing the reaction time and temperature, do not affect the morphology of the produced samples. However, Fig. 3(a,b,d,e,f) show mainly agglomerated nanoparticles. Whiles, Fig. 3c shows individual particles for sample prepared at 140 ˚C for 12 h

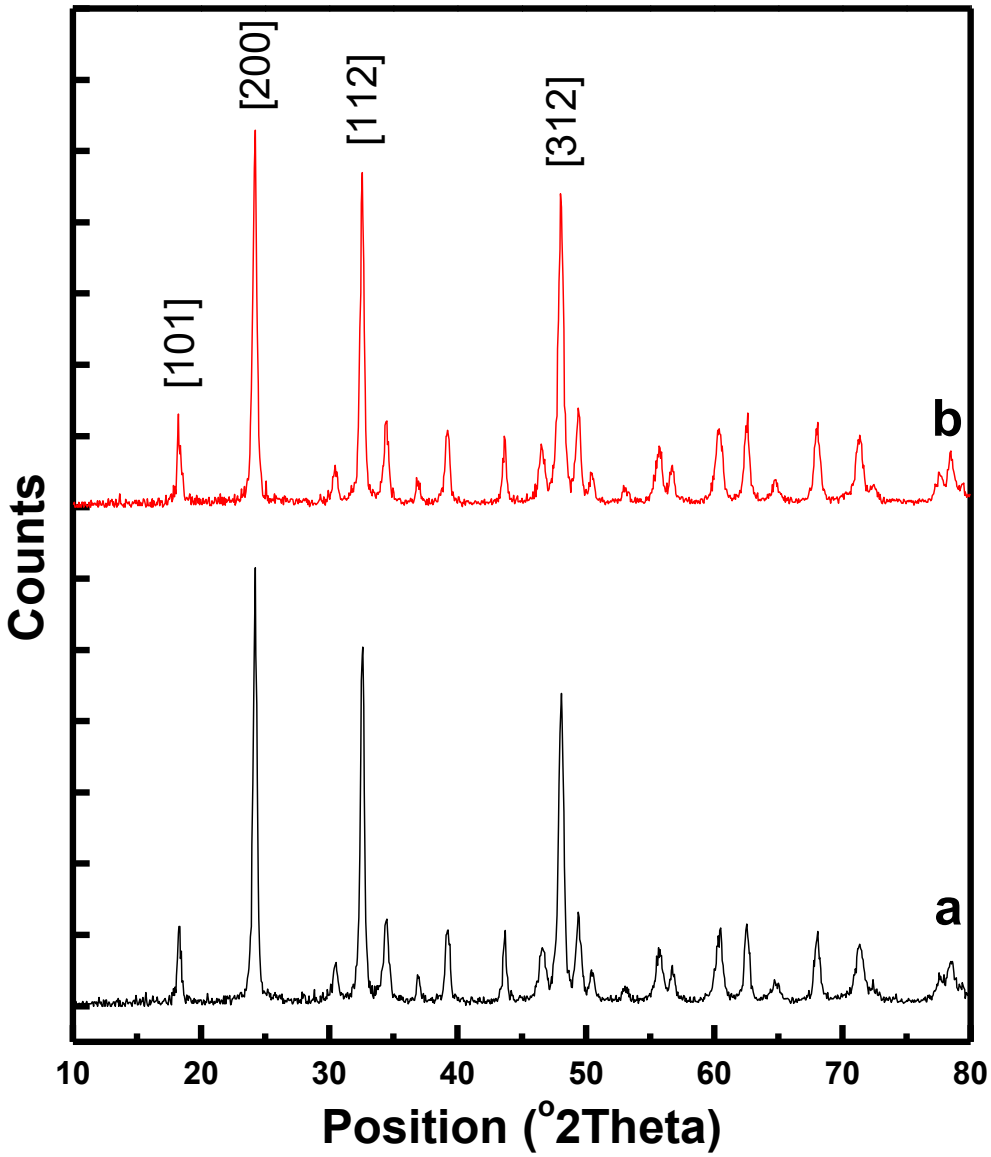

Fig. 4. XRD pattern of a) $CeVO_4$ and b) $Ce_{0.96}VO_4$:$Dy_{0.04}$ NPs.

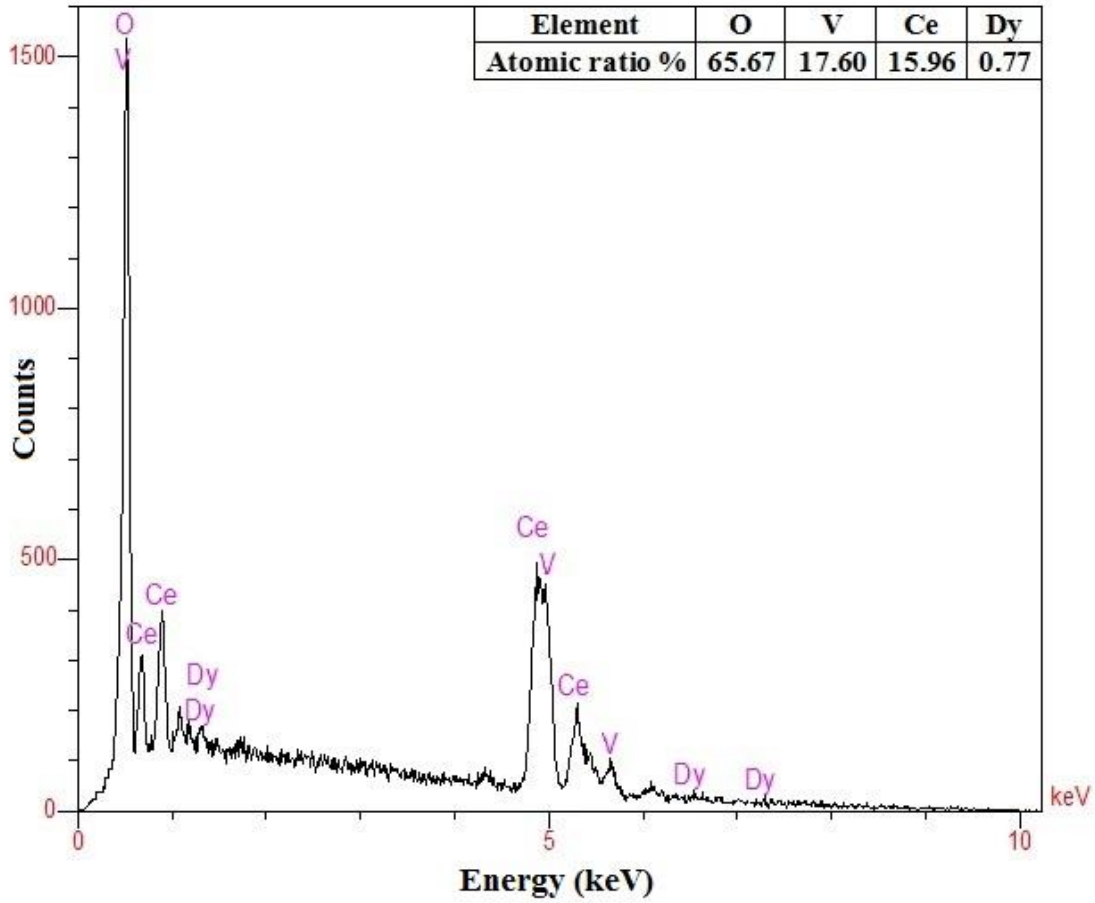

Fig. 5. EDAX pattern of $CeVO_4$:Dy^{3+} NPs.

and this sample has better morphology.

Fig. 4 shows XRD pattern of $Ce_{0.96}VO_4$:$Dy_{0.04}$ nanoparticles compared to pure $CeVO_4$ NPs. As is obvious, because of low concentration of Dy, there is no impurity effect in XRD pattern. The energy dispersive X-ray spectroscopy was performed to verify the existence of Dy as impurity. EDAX pattern of $CeVO_4$:Dy^{3+} along with atomic percentages shown in Fig. 5, demonstrates that there exist only elements Ce, V, O and Dy. So, the EDAX pattern confired that Dy^{3+} ions with concentration of 0.77 % are located in crystalline lattice. Absence of N or C signals in the EDAX spectrum indicates that the sample is devoid of Brij 35. The SEM and TEM images of $CeVO_4$:Dy^{3+} NPs are shown in Fig. 6(a,b), respectively. As shown in Fig. 6a, there is no obvious difference in the shape and size of nanoparticles between doped and pure $CeVO_4$. Fig.6b shows that some $CeVO_4$:Dy^{3+} NPs are spherical in shape and others tend to be rod-like with different sizes.

To study the effect of annealing temperature on crystalline and photolominescence properties, $Ce_{0.96}VO_4$:$Dy_{0.04}$ nanocrystals were calcined at 300, 500, 700 and 900 °C. Fig. 7 shows the XRD patterns of $Ce_{0.96}VO_4$:$Dy_{0.04}$ NPs annealed at 500, 700 and 900 °C. Fig. 7(a-c) indicate the tetragonal phase of $CeVO_4$ with the standard pattern (JCPDS 84-1457). The peak intensity becomes weaker with raising the calcination temperature from 500 to 900 °C, implying that the amorphous phase is increasing.

The UV-visible absorption spectra of the synthesized $CeVO_4$ nanocrystals are shown in Fig. 8A. As a result of dispersing the product in ethanol and sonicating the mixture for 5 min, the clear solution is formed. Considering that the light absorption is related to the host lattice, this analysis describes only $CeVO_4$ without impurity [35]. The optical absorption of the film shows that the absorption increases abruptly in wavelengths

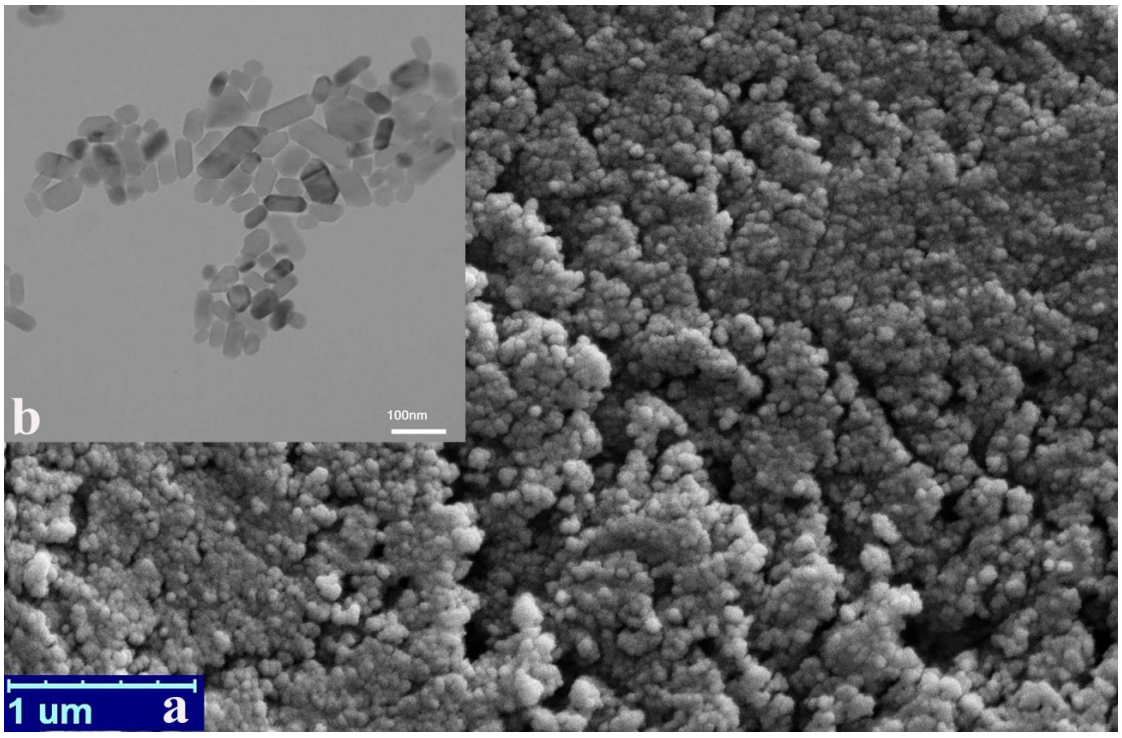

Fig. 6. (a) SEM and (b) TEM images of $CeVO_4$:Dy^{3+} NPs.

below 400 nm and has a peak at 286 nm. These prominent peaks were attributed to the UV absorption of the VO_4^{3-} of rare earth vanadates. These attributed to the charge transfer from the oxygen ligands to the central vanadium atoms inside the VO_4^{3-} groups of cerium orthovanadate [36]. The optical band gap of the nanoparticles was investigated using the optical absorption spectra. The produced nanoparticles have direct band gap, therefore Eq. (1) was utilized for estimating the band gap [37]. The absorption coefficient α is related to the band gap E_g as [26]:

$$\alpha h\nu = B(h\nu - E_g)^{1/2} \quad (1)$$

Where hν is the energy of the photon. The absorption coefficient α has been calculated from the optical absorption using the relation α = (l/t) log (absorption). The optical band gap E_g was determined by extrapolating the linear portion of the plot relating $(\alpha h\nu)^2$ and hν to $(\alpha h\nu)^2 = 0$ [38]. Therefore, the optical band gap value was estimated 3.88 ev, according to Fig. 8B.

The optical properties of $CeVO_4$:Dy^{3+} were examined using PL spectroscopy. PL spectrum of a material indicates its capability to emit photons and were used to illustrate the down conversion process. Fig. 9 show the emission spectra of $CeVO_4$:Dy^{3+} nanocrystals with different Dy^{3+} concentrations, while dispersed in water and following excitation at 280 nm. According to the emission spectra, pure $CeVO_4$ and $CeVO_4$:Dy^{3+} emit lines ranging from 400 – 550 nm with PL peaks located at 455 and 481 nm, respectively. They could be specified as the electronic transitions from the lowest excited states arising from $5d^1$ to the $4f^1$ ground state ($^2F_{5/2}$ and $^2F_{7/2}$) of the Dy^{3+} ions [36] and illustrate charge transfer transition in the V-O band. As can be seen, the different concentration of impurity just changes the PL intensity and not the location of PL peaks because the dopant did not change the crystal structure. Fig. 10 shows the PL intensity of $CeVO_4$:Dy^{3+} NPs as a function of impurity concentration. According to the emission spectra, the PL intensity of $Ce_{1-x}VO_4$:Dy_x is optimized at 0.04 mmol concentration of impurity. However, the PL properties modified with enhancement Dy^{+3} concentration because of enhanced V-V separation after increment the activator in host lattice. But excessive amount of dopant filled the fluorescence quenching sites, and decrease the emission intensity. The increment of PL intensity

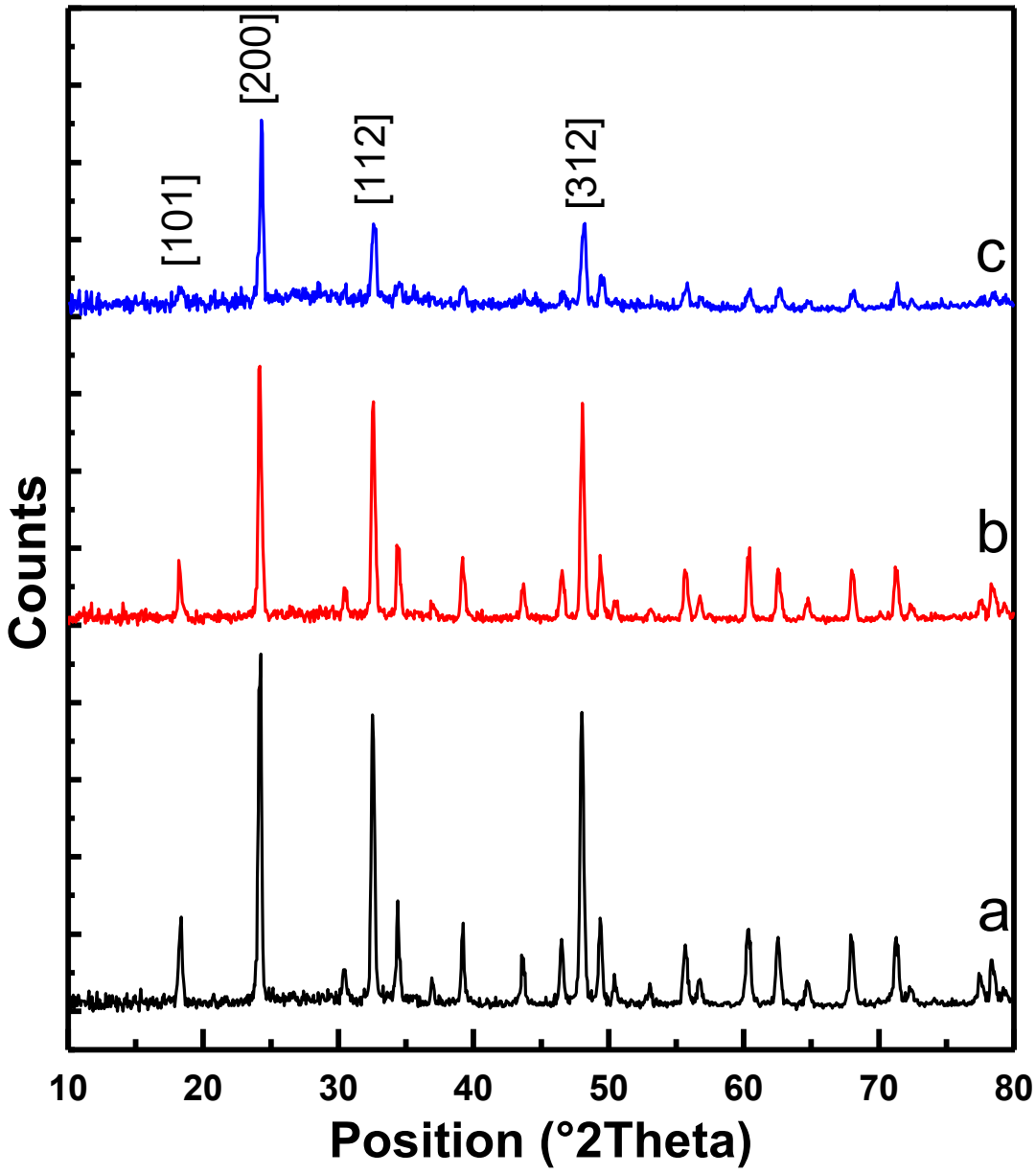

Fig. 7. XRD pattern of $CeVO_4$ NPs annealed. a) 500, b) 700, c) 900°C.

confirms the ability of Dy^{3+} in down converting the excited UV light to visible light. Furthermore, the effect of annealing temperature on intensity of PL spectra of $Ce_{0.96}VO_4$:$Dy_{0.04}$ NPs was studied. The PL intensity of the prepared samples annealed at different temperatures, under 280 nm excitation presented in Fig. 11. As can be seen, the emission intensity decreased with increasing the annealing temperature from 300 to 900 ˚C. It might be due to result of deterioration crystallinity and increased lattice defects. The results of PL properties of $CeVO_4$:$Dy_{0.04}$ nanocrystals demonstrate the down conversion mechanism from UV light to visible light and this sample is best choice. Fig. 12 shows a schematic energy-level diagram of down conversion process of $CeVO_4$:Dy nanocrystals. It is expected that DSSC efficiency improved with this down converter layer.

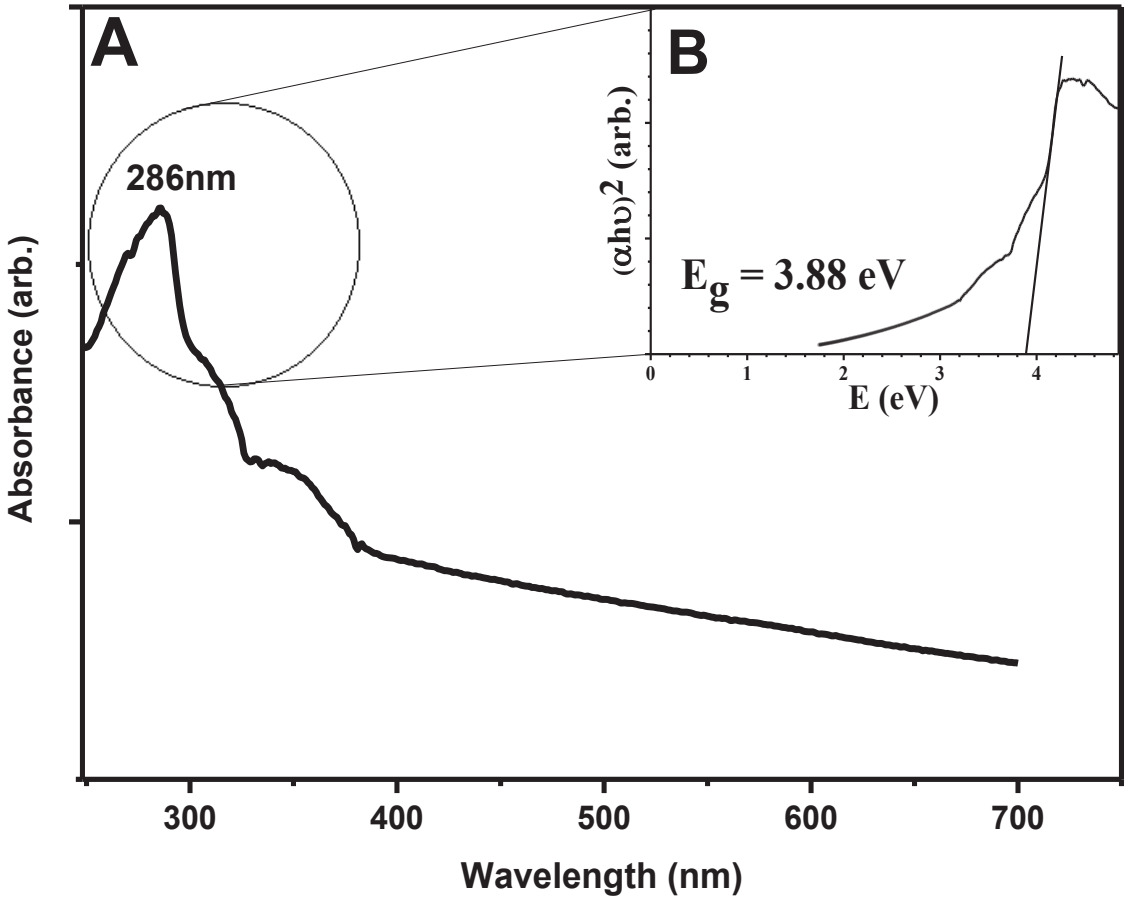

Fig. 8. (A) the absorption spectra of $CdVO_4$ NPs (B) extrapolating the linear portion of the plot relating $(\alpha h\nu)^2$ and $h\nu$ to $(\alpha h\nu)^2 = 0$ that determines the optical band gap E_g.

Using DC material in DSSC

TiO_2 EPs Fabrication and solar cell assembly

Electrophoresis deposition (EPD) was utilized for preparing PEs applied in DSSCs. In EPD, charged powder particles, dispersed or suspended in a liquid medium are attracted and deposited onto a conductive substrate of opposite charge on application of a DC electric field [39]. A mixture of TiO_2 nanopowders (P25), acetone, acetyl acetone, I_2, DI water, and ethanol was stirred for 24 h and used as electrophoretic suspension liquid. For the electrophoresis experiment, the cathode (a pure steel mesh) and anode (the cleaned FTO glass) are placed in a EPD solution with a distance between two electrodes about 1 cm. The EPD voltage is set 10 V. The deposition cycles 6 times which each one takes 5 s. The coated substrates heated at 150 °C while they were in touch with air about 5 min. Final thickness was about 15 µm. The resulting layer was annealed at 500 °C in air for 15 min. Afterward, for sensitization purpose, the fabricated electrodes immersed into N719 dye solution in ethanol and acetonitrile (0.03 mM) for 24 h. a Pt coated FTO glass was used as a counter electrode. Two electrodes were sandwiched by using a polymer spacer (surlyn) and then the electrolyte containing I^-/I_2^- redox couple was injected into the cell.

To study the effect of $Ce_{0.96}VO_4$:$Dy_{0.04}$ on performance of DSSC, the prepared NPs used through two ways, inside and outside the dye sensitized solar cell. For inside use, the NPs were added to the electrophoretic suspension liquid with different molar concentration in the first layer of photoelectrode. For outside use, a spin coating process was used to obtain an uniform thin film of $CeVO_4$:Dy NPs on the back surface of photo

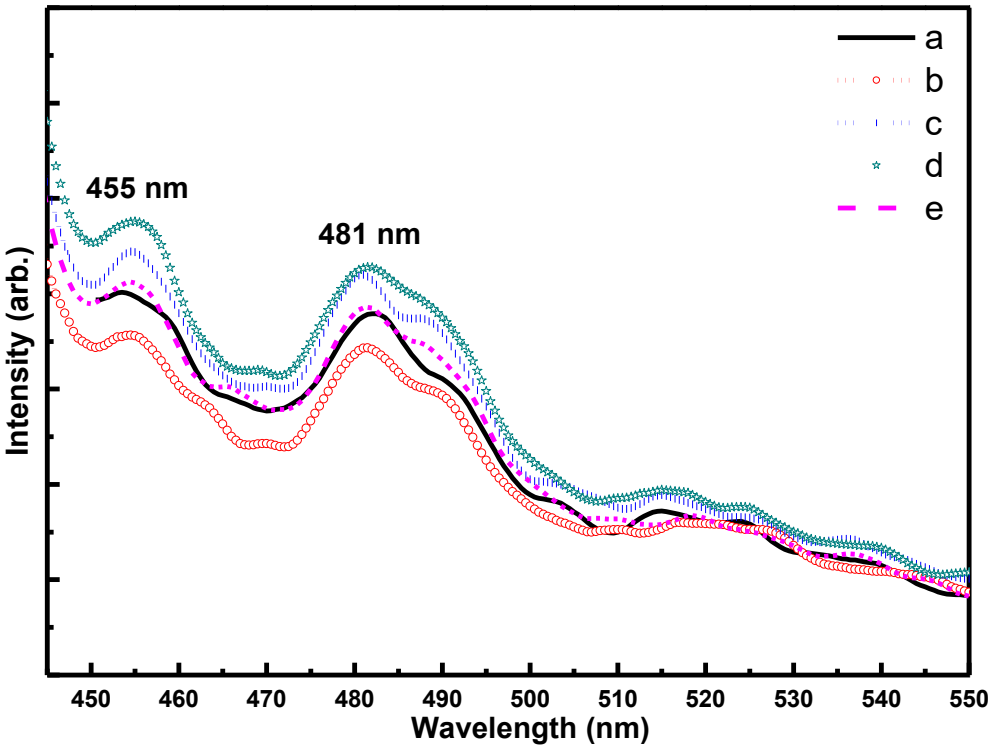

Fig. 9. The emission spectra of $Ce_{1-x}VO_4$: : (a) x=0.00, (b) x=0.01, (c) 0.02, (d) x=0.04, (e) x=0.06

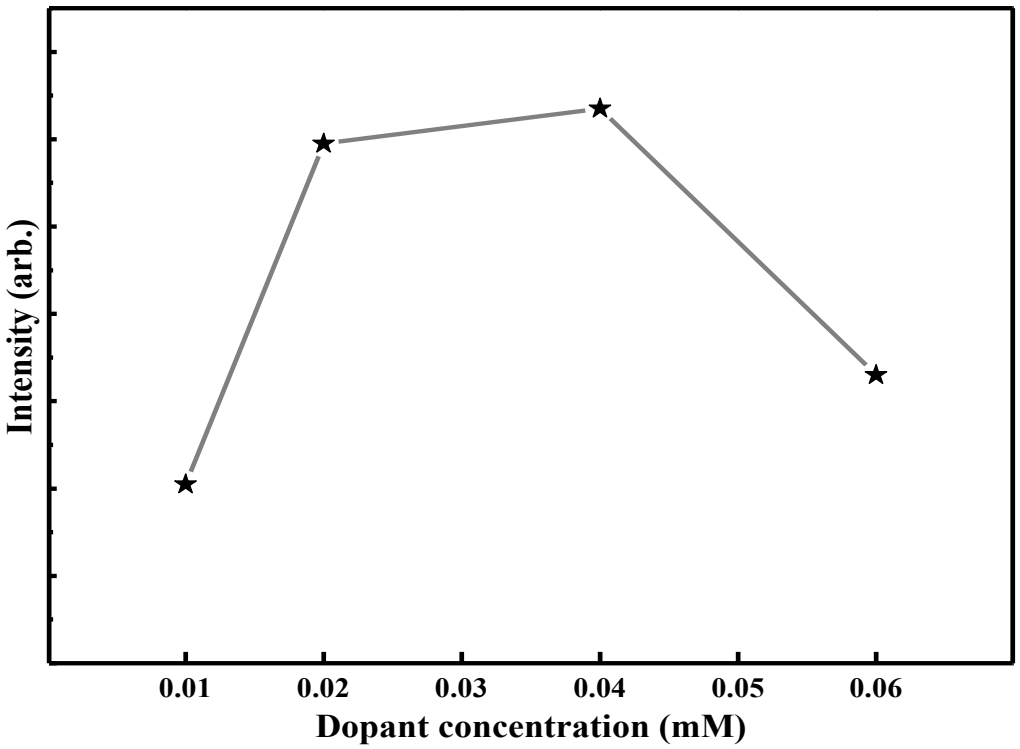

Fig. 10. The PL intensity of $CeVO_4$:Dy^{3+} NPs as a function of dopant concentration.

electrode.

Photovoltaic performance of the DSSCs

The optical properties indicate that $Ce_{0.96}VO_4:Dy_{0.04}$ NPs is a good candidate for DSSC as DC material that could absorb UV light and emit visible light. Photovoltaic experiments were performed in a standard system. Corresponding

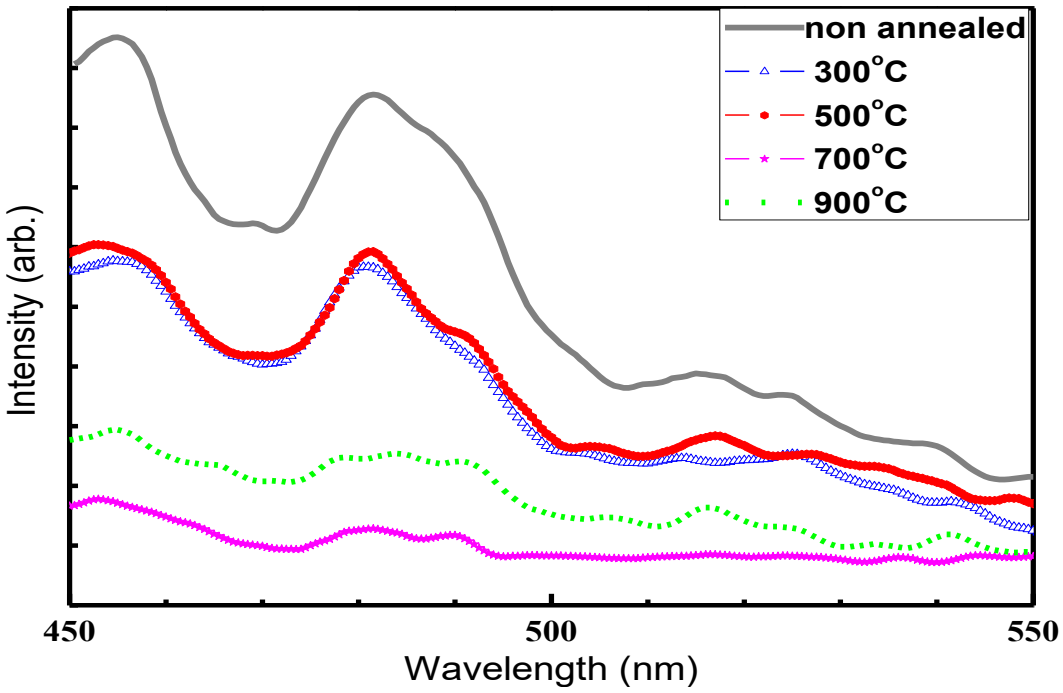

Fig. 11. PL spectra of annealed $Ce_{0.96}VO_4:Dy_{0.04}$ NPs.

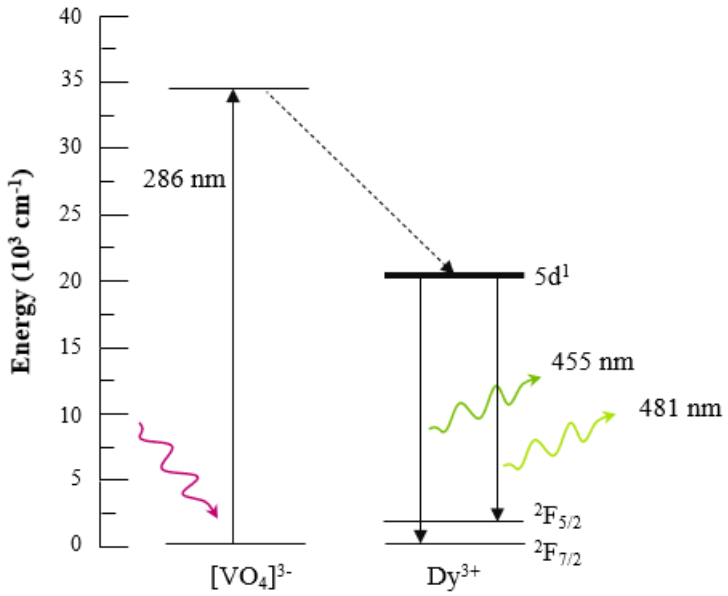

Fig. 12. Schematic energy-level diagram of $CeVO_4:Dy^{3+}$ NPs showing the concept of down conversion process.

photovoltaic characteristics are summarized in table 2. Depicted in Fig. 13 is the I-V characteristics of DSSCs for PE without $CeVO_4$:Dy^{3+} NPs and with different concentration of $CeVO_4$:Dy^{3+} NPs. With a look at table 2, it reveals that devices with DC NPs concentration exceeding 1%, go through efficiency reduction in DSSC. The reasons for this reduction is extra replacement of $CeVO_4$;Dy^{3+} instead of TiO_2 which decreases the absorption of dye. According to table 2, by reducing the concentration of DC

Table 2. Photovoltaic characteristics of the fabricated of DSSCs.

Device. no	Condition	Concentration	J_{sc} (mA/cm)	V_{oc} (V)	FF	η (%)
1	standard	0	18.76	0.69	0.53	6.83
2	back surface of the PE	0.1 M	19.84	0.67	0.55	7.38
3	back surface of the PE	0.3 M	17.39	0.69	0.45	5.35
4	used to prepare the PE	0.5%	18.18	0.71	0.56	7.21
5	used to prepare the PE	1%	16.66	0.69	0.56	6.47
6	used to prepare the PE	4%	12.49	0.75	0.54	5.04

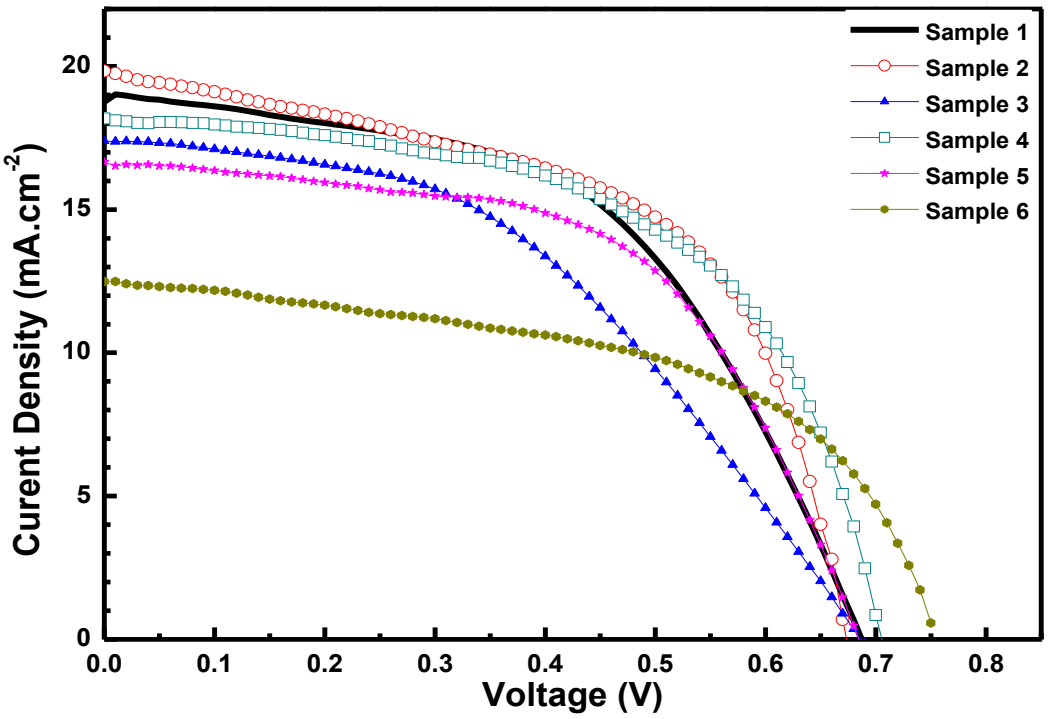

Fig. 13. The photocurrent-voltage curves of dye-sensitized solar cells.

NPs' to 0.5 %, the photovoltaic characteristics is improved compare to DSSC lacking DC NPs. This DSSC had short current density (J_{sc}) of 18.18 $mA.cm^{-2}$, Fill Factor (FF) of 0.56, open circuit voltage ($V_{oc)}$ of 0.71 V and energy efficiency (η) of 7.21%, while the DSSC lacking DC NPs had J_{sc} of 18.76 $mA.cm^{-2}$, FF of 0.53, V_{oc} of 0.67 V and efficiency of 6.83%. Therefore, PE with 0.5% concentration of DC NPs causes the FF and energy conversion efficiency to increase by 5.66% and 5.56% respectively. This increment of FF is due to increase in J_{mpp} and also small reduction of J_{sc} which cause an increase in efficiency of DSSC. If the level of DC material concentration cuts down, its role as UV filter will be lost. For device 2, According to Fig. 13, luminescent film coated at the back surface of PE with concentration of 0.1 M, causes the current density and energy conversion efficiency to improve respectively by 5.76% and 8.05% compared to the uncoated solar cell. Device 2 has J_{sc} of 19.84 $mA.cm^{-2}$, FF of 0.55, V_{oc} of 0.67 V and η of 7.38% as photovoltaic characteristics, because the emitted light by down-converter is capable to be reabsorbed by N719 dye and generate current. The presence of $CeVO_4:Dy^{3+}$ NPs on the surface of DSSC yields the incident single UV photon to convert to two visible photons. This mechanism leads to increase in photon flux and current density and it is clear that increase in current density improves the efficiency.

On the other hand, the solar cell coated with luminescent film with concentration of 0.3 M, reduces the current density and energy conversion efficiency by 7.3% and 21.67% respectively. More increase in concentration of luminescent film, leads to more chance for reflection of the incident light. Considering the above outcome, the DC material used in the cell and near the cell surface has the optimum performance and is recommended for DSSCs.

CONCLUSION

In conclusion, for the first time, $CeVO_4:Dy$ nanocrystals employ for improving DSSC as alight converter. $Ce_{0.96}VO_4:Dy_{0.04}$ NPs were synthesized by hydrothermal method in optimized condition of 140˚ C for 12 h. SEM analysis showed that the produced particles are uniform with the spherical shape and average diameter ranging from 20-40 nm. UV-vis and PL studies indicated that $Ce_{0.96}VO_4:Dy_{0.04}$ NPs can act as down conversion (DC) material, that is absorb UV light and emit visible light. In this paper, the used thin film of $CeVO_4:Dy^{3+}$ NPs as DC layer led to improved fill factor, current density and efficiency for DSSC. Utilizing a layer of $CeVO_4:Dy^{3+}$ NPs on the back surface of the PE resulted in enhancement of DSSC efficiency by a factor of 5.56% and use them inside the PE caused the efficiency to increase by 8.05%.

ACKNOWLEDGEMENT

The research council of the University of Kashan is gratefully acknowledged for financial support of this work.

CONFLICT OF INTEREST

The authors declare that there is no conflict of interests regarding the publication of this manuscript.

REFERENCES

1. Nayak SK, Panda SK, Das S. Renewable Energy-Based Resource Management in Cloud Computing: A Review. Lecture Notes in Networks and Systems: Springer Singapore; 2020. p. 45-56.
2. Semieniuk G, Taylor L, Rezai A, Foley DK. Plausible energy demand patterns in a growing global economy with climate policy. Nature Climate Change. 2021;11(4):313-318.
3. Siah Chehreh Ghadikolaei S. An enviroeconomic review of the solar PV cells cooling technology effect on the CO_2 emission reduction. Solar Energy. 2021;216:468-492.
4. Siah Chehreh Ghadikolaei S. Solar photovoltaic cells performance improvement by cooling technology: An overall review. Int J Hydrogen Energy. 2021;46(18):10939-10972.
5. de la Cruz RM, Kanyinda-Malu C, Santiuste JEM. Design of GaAs nanowires array based photovoltaic solar cells: Simulations of optical reflectance. Physica B: Condensed Matter. 2021;619:413233.
6. Rabaia MKH, Abdelkareem MA, Sayed ET, Elsaid K, Chae K-J, Wilberforce T, et al. Environmental impacts of solar energy systems: A review. Sci Total Environ. 2021;754:141989.
7. Mahalingam S, Manap A, Omar A, Low FW, Afandi NF, Chia CH, et al. Functionalized graphene quantum dots for dye-sensitized solar cell: Key challenges, recent developments and future prospects. Renewable and Sustainable Energy Reviews. 2021;144:110999.
8. Devadiga D, Selvakumar M, Shetty P, Santosh MS. Recent progress in dye sensitized solar cell materials and photo-supercapacitors: A review. J Power Sources. 2021;493:229698.
9. Faraz SM, Mazhar M, Shah W, Noor H, Awan ZH, Sayyad MH. Comparative study of impedance spectroscopy and photovoltaic properties of metallic and natural dye based dye sensitized solar cells. Physica B: Condensed Matter. 2021;602:412567.
10. Sheikh MS, Roy A, Dutta A, Sundaram S, Mallick TK, Sinha TP. Nanostructured perovskite oxides for dye-sensitized solar cells. J Phys D: Appl Phys. 2021;54(49):493001.
11. Selvapriya R, Abhijith T, Ragavendran V, Sasirekha V, Reddy

VS, Pearce JM, et al. Impact of coupled plasmonic effect with multishaped silver nanoparticles on efficiency of dye sensitized solar cells. J Alloys Compd. 2022;894:162339.
12. Pakravesh F, Izadyar M, Arkan F. Effect of electron donor and acceptor on the photovoltaic properties of organic dyes for efficient dye-sensitized solar cells. Physica B: Condensed Matter. 2021;609:412815.
13. Hosseinpanahi K, Golzarian MR, Abbaspour-Fard MH, Feizy J. Improving The Efficiency of DSSC with A Novel Multi-dye layers Approach. Optik. 2020;208:164068.
14. Selvanathan V, Yahya R, Shahiduzzaman M, Ruslan MH, Muhammad G, Amin N, et al. Ionic liquid infused starch-cellulose derivative based quasi-solid dye-sensitized solar cell: exploiting the rheological properties of natural polymers. Cellulose. 2021.
15. Sasikala R, Kandasamy M, Suresh S, Ragavendran V, Sasirekha V, Pearce JM, et al. Enhanced dye-sensitized solar cell performance using strontium titanate perovskite integrated photoanodes modified with plasmonic silver nanoparticles. J Alloys Compd. 2021;889:161693.
16. Rajeswari R, Susmitha K, Jayasankar CK, Raghavender M, Giribabu L. Enhanced light harvesting with novel photon upconverted Y_2CaZnO_5:Er^{3+}/Yb^{3+} nanophosphors for dye sensitized solar cells. Solar Energy. 2017;157:956-965.
17. Ko SH, Lee D, Kang HW, Nam KH, Yeo JY, Hong SJ, et al. Nanoforest of Hydrothermally Grown Hierarchical ZnO Nanowires for a High Efficiency Dye-Sensitized Solar Cell. Nano Lett. 2011;11(2):666-671.
18. Han L, Islam A, Chen H, Malapaka C, Chiranjeevi B, Zhang S, et al. High-efficiency dye-sensitized solar cell with a novel co-adsorbent. Energy & Environmental Science. 2012;5(3):6057.
19. Qin Y, Hu Z, Lim BH, Chang WS, Chong KK, Zhang P, et al. Sol-hydrothermal synthesis of TiO 2 :Sm^{3+} nanoparticles and their enhanced photovoltaic properties. J Alloys Compd. 2016;686:803-809.
20. Chang H, Chen C-H, Kao M-J, Chien S-H, Chou C-Y. Photoelectrode thin film of dye-sensitized solar cell fabricated by anodizing method and spin coating and electrochemical impedance properties of DSSC. Appl Surf Sci. 2013;275:252-257.
21. Chen T, Shang Y, Hao S, Tian L, Hou Y, Yang C. Enhancement of dye sensitized solar cell efficiency through introducing concurrent upconversion/downconversion core/shell nanoparticles as spectral converters. Electrochimica Acta. 2018;282:743-749.
22. Yao N, Huang J, Fu K, Liu S, E D, Wang Y, et al. Efficiency enhancement in dye-sensitized solar cells with down conversion material ZnO: Eu^{3+}, Dy^{3+}. J Power Sources. 2014;267:405-410.
23. Teymourinia H, Salavati-Niasari M, Amiri O, Farangi M. Facile synthesis of graphene quantum dots from corn powder and their application as down conversion effect in quantum dot-dye-sensitized solar cell. J Mol Liq. 2018;251:267-272.
24. Shen LF, Chen BJ, Pun EYB, Lin H. Sm3+-doped alkaline earth borate glasses as UV→visible photon conversion layer for solar cells. J Lumin. 2015;160:138-144.
25. Li H, Wang X, Ohulchanskyy TY, Chen G. Lanthanide-Doped Near-Infrared Nanoparticles for Biophotonics. Adv Mater. 2020;33(6):2000678.
26. Risha Y, Susevski V, Hüttmann N, Poolsup S, Minic Z, Berezovski MV. Proteome of breast cancer derived microvesicles. Siberian Medical Review. 2021(2):68-71.
27. Chen J, Huang X, Wang L, Zhang Q. Preparation and properties of Nd:YAG ultra-fine powders. Journal of Rare Earths. 2011;29(1):44-47.
28. Jia H, Li X, An X, Chang S, Liu Z, Peng F, et al. Enhanced Capture of Broadband Solar-Blind UV Light via Introducing Alkali-Metal Ions (Li^+ , Na^+ , and K^+) into DC Spectral Converter. Advanced Optical Materials. 2020;9(6):2001703.
29. Jia H, Zhou Y, Wang X, Zhang W, Feng X, Li Z, et al. Luminescent properties of Eu-doped magnetic Na_3FeF_6. RSC Advances. 2018;8(67):38410-38415.
30. Jia H, Liu Z, Liao L, Gu Y, Ding C, Zhao J, et al. Upconversion Luminescence from $Ln^{3+}$$Ho^{3+}$,$Pr^{3+}$) Ion-Doped $BaCl_2$ Particles via NIR Light of Sun Excitation. The Journal of Physical Chemistry C. 2018;122(17):9606-9610.
31. Jia H, Zhou Y, Li X, Li Y, Zhang W, Fu H, et al. Synthesis and phase transformation of $NaGdF_4$:Yb–Er thin films using electro-deposition method at moderate temperatures. CrystEngComm. 2018;20(43):6919-6924.
32. Kalai Selvan R, Gedanken A, Anilkumar P, Manikandan G, Karunakaran C. Synthesis and Characterization of Rare Earth Orthovanadate (RVO_4; R = La, Ce, Nd, Sm, Eu & Gd) Nanorods/Nanocrystals/Nanospindles by a Facile Sonochemical Method and Their Catalytic Properties. J Cluster Sci. 2008;20(2):291-305.
33. Khachatourian AM, Golestani-Fard F, Sarpoolaky H, Vogt C, Vasileva E, Mensi M, et al. Microwave synthesis of Y_2O_3:Eu^{3+} nanophosphors: A study on the influence of dopant concentration and calcination temperature on structural and photoluminescence properties. J Lumin. 2016;169:1-8.
34. Nguyen T-D, Dinh C-T, Do T-O. Monodisperse Samarium and Cerium Orthovanadate Nanocrystals and Metal Oxidation States on the Nanocrystal Surface. Langmuir. 2009;25(18):11142-11148.
35. Ronda CR. Phosphors for lamps and displays: an applicational view. J Alloys Compd. 1995;225(1-2):534-538.
36. Ekthammathat N, Thongtem T, Phuruangrat A, Thongtem S. Synthesis and Characterization of $CeVO_4$ by Microwave Radiation Method and Its Photocatalytic Activity. Journal of Nanomaterials. 2013;2013:1-7.
37. Callaway J. Radiative recombination of electrons with hydrogen atoms. Phys Lett A. 1974;48(5):359-360.
38. Kamalasanan MN, Deepak Kumar N, Chandra S. Structural, optical, and dielectric properties of sol-gel derived $SrTiO_3$ thin films. J Appl Phys. 1993;74(1):679-686.
39. Besra L, Liu M. A review on fundamentals and applications of electrophoretic deposition (EPD). Prog Mater Sci. 2007;52(1):1-61.